

The FUSE Spectrum of PG 0804 +761: A Study of Atomic and Molecular Gas in the Lower Galactic Halo and Beyond

Philipp Richter, Blair. D. Savage, Bart P. Wakker

Washburn Observatory, University of Wisconsin-Madison, 475 N. Charter Street, Madison, WI 53706

richter@astro.wisc.edu, savage@astro.wisc.edu, wakker@astro.wisc.edu

Kenneth R. Sembach

Department of Physics and Astronomy, Johns Hopkins University, 3400 N. Charles Street, Baltimore MD 21218

sembach@pha.jhu.edu

and

Peter M.W. Kalberla

Universität Bonn, Radioastronomisches Institut, D-53121 Bonn, Germany

kalb@astro.uni-bonn.de

ABSTRACT

We present an analysis of interstellar and intergalactic absorption lines in the FUSE spectrum of the low-redshift quasar PG 0804 +761 ($z_{\text{em}} = 0.100$) at intermediate resolution (FWHM ~ 25 km s $^{-1}$) in the direction $l = 138^\circ.3$, $b = 31^\circ.0$. With a good signal-to-noise ratio (S/N) and the presence of several interesting Galactic and extragalactic absorption components along the sight line, this spectrum provides a good opportunity to demonstrate the ability of FUSE to do both interstellar and extragalactic science. Although the spectrum of PG 0804 +761 is dominated by strong absorption from local Galactic gas at 0 km s $^{-1}$, we concentrate our study on absorption by molecular hydrogen and neutral and ionized metals related to an intermediate-velocity cloud (IVC) in the lower Galactic halo at -55 km s $^{-1}$, and on absorption from O VI extended to negative velocities. In the IVC, weak molecular hydrogen absorption is found in 5 lines for rotational levels 0 and 1, leading to a total H $_2$ column density of $\log N = 14.71 \pm 0.30$. We derive an O I gas-phase abundance for the IVC of $1.03^{+0.71}_{-0.42}$ solar. Lower abundances of other elements (Fe, Si) imply depletion onto dust grains or the presence of higher, undetected ionization states. The presence of N II and Fe III absorption at -55 km s $^{-1}$ indicates that a fraction of the hydrogen is ionized. From the relative abundances of O I and P II we estimate a degree of ionization $\text{H}^+ / (\text{H}^0 + \text{H}^+)$ of ~ 19 percent. Absorption by O VI is found at velocities as negative as -110 km s $^{-1}$, but no absorption from any species is found at velocities of ~ -180 km s $^{-1}$ where absorption from the nearby high-velocity cloud Complex A would be expected. We suggest that the extended O VI absorption traces hot gas situated above the Perseus spiral arm. Finally, we find intergalactic absorption by an intervening H I Ly β absorber at $z_{\text{abs}} = 0.019$ and absorption by H I, C III and O VI in an associated system at $z_{\text{abs}} = 0.102$. No intervening O VI absorbers are seen in the spectrum of PG 0804 +761.

Subject headings: ISM: clouds – ISM: abundances – quasars: absorption lines – quasars: individual (PG 0804 +761) – Galaxy: halo

1. Introduction

The successful launch of the *Far Ultraviolet Spectroscopic Explorer* (FUSE) in June 1999 (Moos et al. 2000) has provided a major new facility for obtaining absorption line spectra at intermediate resolution (FWHM $\sim 25 \text{ km s}^{-1}$) in the far ultraviolet (FUV) regime from 905 to 1187 Å. In this wavelength range, many spectral diagnostic lines provide information over a wide range of physical conditions found in the diffuse and translucent interstellar medium. The Lyman and Werner bands of molecular hydrogen (H_2), as well as absorption bands of carbon monoxide (CO), give important information about the cold molecular gas. The complete Lyman series of neutral hydrogen and deuterium, in combination with a large number of transitions of neutral and weakly ionized metals, can be used to study the conditions of the neutral and diffuse ionized gas in great detail. Finally, absorption lines from highly ionized species, in particular the O VI doublet near 1030 Å, are excellent tracers of the hot component of the ISM, as found in halos of galaxies or within expanding shells and superbubbles. Absorption spectroscopy in the FUV range is an extremely powerful technique for the study of the multi-phase structure of the ISM of the Milky Way and gives additional information about the structure and physics of the intergalactic medium (IGM), when applied to quasars or Active Galactic Nuclei (AGNs).

FUV absorption spectroscopy with the *Copernicus* satellite (1972-1981) was performed to intensively study the interstellar medium (for a review see Spitzer & Jenkins 1975), but was limited in sensitivity to nearby bright stars as background sources. Later satellites, such as the *International Ultraviolet Explorer* (IUE) and the *Hubble Space Telescope* (HST), did not cover wavelengths below 1150 Å. The *Orbiting and Retrievable Far and Extreme Ultraviolet Spectrometer* (ORFEUS), launched in 1996 for a 14-day *Space Shuttle* mission, was able to obtain intermediate resolution FUV spectra toward extragalactic background sources. Observations with ORFEUS led to many new insights concerning the ISM in the Galactic halo and the Magellanic Clouds (Widmann et al. 1998; de Boer et al. 1998; Richter et al. 1998, 1999), but the number of observed objects was limited due to the short mission duration. With FUSE, the number of extragalactic sight-line spectra in the FUV range is growing rapidly and the very first results from FUSE (e.g., Oegerle et al. 2000, Savage et al. 2000; Sembach et al. 2000; Shull et al. 2000; Snow et al. 2000) already imply that the satellite will make important contributions to studies of the ISM and IGM. With its high sensitivity and its moderate resolution, FUSE is able to obtain spectra toward fainter (and thus more distant) background sources and so gives access to regions in space which could not be studied before in the FUV range.

In this paper we present measurements of absorption lines in the spectrum of the bright low-redshift quasar PG 0804+761 ($V = 15.20$, $z_{\text{em}} = 0.100$, Schmidt & Green 1983) obtained with FUSE in January 2000. The line of sight to PG 0804+761 in the Galactic direction $l = 138^\circ.3$, $b = +31^\circ.0$ passes through local Galactic gas and through the Galactic halo above nearby and distant spiral arms. The FUSE spectrum of PG 0804+761 thus provides an opportunity to investigate the ISM along a path extending over the outer regions of the Milky Way. The goal of this paper is to analyze the sight-line structure in this interesting direction and to provide a reference spectrum for further studies.

The outline of this paper is as follows: a review of the sight-line structure is given in §2. In §3 we present the FUSE observations and the data reduction. Absorption by local Galactic gas is briefly discussed in §4. Absorption by molecules, neutral and weakly ionized species at intermediate negative velocities is presented in §5, while absorption by moderately and highly ionized gas is described in §6. In §7 we shortly discuss the lack of absorption by high-velocity gas from Complex A. §8 presents the results for the intergalactic gas and the associated system in front of PG 0804+761. Finally, a summary of our study is given in §9.

2. The Sight-line Structure toward PG 0804+761

The absorption along the line of sight to PG 0804+761 ($l = 138^{\circ}.3, b = +31^{\circ}.0$) is primarily dominated by various Galactic disk and halo gas-components. The sight line passes through local Galactic gas, through intermediate-velocity gas in the Galactic halo and over the outer spiral arms of the Milky Way. The position of PG 0804+761 lies $< 0^{\circ}.5$ off the edge of high-velocity cloud Complex A (as seen in 21 cm; Wakker & van Woerden 1997), so that weak absorption from the outermost edge of Complex A could be present in spectrum of PG 0804+761. In the direction $l = 138^{\circ}.3, b = 31^{\circ}.0$ differential Galactic rotation has a systematic influence on the radial velocities. In particular, if halo gas is co-rotating with the underlying disk, velocities in the range 0 to -55 km s^{-1} are predicted for gas with $z < 5 \text{ kpc}$, assuming a flat rotation curve for the outer Galaxy and a LSR rotation speed of 220 km s^{-1} . Additional intergalactic absorption features are expected as well, given the redshift of $z_{\text{em}} = 0.100$ for PG 0804+761.

In this study, we concentrate on absorption associated with the gas at intermediate velocities around -55 km s^{-1} . This component is part of the “Low-Latitude Intermediate-Velocity Arch” (LLIV Arch) defined in HI 21 cm emission (Kuntz & Danly 1996). It is a $5 - 10^{\circ}$ wide, elongated structure, running from $(l,b) \sim (115^{\circ}, 37^{\circ})$ to $(l,b) \sim (165^{\circ}, 35^{\circ})$, and having velocities in the range -30 to -70 km s^{-1} . Fig. 1 shows an HI contour map of the gas in this velocity range, based on data in the Leiden-Dwingeloo Survey (Hartmann & Burton 1997). Six cores are labeled LLIV1 to LLIV6, as defined by Kuntz & Danly (1996). The contours show the high-velocity gas at $v_{\text{LSR}} < -100 \text{ km s}^{-1}$ in this region of the sky. A distance bracket for the LLIV Arch of $0.9-1.8 \text{ kpc}$ ($z=0.6-1.2 \text{ kpc}$) is determined by Wakker (2000), using the detection of Ca II and Mg II absorption at its velocity in four background horizontal branch stars, combined with significant non-detections of Ca II and Mg II in three other stars (Vladilo et al. 1994; Welsh, Craig & Roberts 1996; Wakker et al. 1996; Ryans et al. 1997). In the Galactic plane the Perseus Arm spans the longitude range of the LLIV Arch. According to Reynolds et al. (1995), this spiral arm lies at a distance of $\sim 2.5 \text{ kpc}$ from the Sun. The LLIV Arch thus appears to lie about 1 kpc above the plane in the inter-arm region between the Perseus and the Local spiral arm. It deviates by about -40 km s^{-1} from the velocity expected for a co-rotating cloud at its position. An approximate metallicity for the LLIV Arch was previously derived from the IUE spectrum of SN 1993 J ($l = 142^{\circ}.2, b = 40^{\circ}.9$; de Boer et al. 1993; Vladilo et al. 1993). In this data, the LLIV Arch shows an abundance pattern typical for warm disk gas (as defined by Savage & Sembach 1996). As Zn II is generally undepleted, its abundance of 1.6 ± 0.4 times solar suggested a slightly supersolar intrinsic abundance for the LLIV Arch.

Two portions of the FUSE spectrum of PG 0804+761 are presented in Fig. 2. The distribution of HI 21 cm emission along the sight line, as measured with the 100 m radio telescope in Effelsberg (Wakker et al. 2000; $9'.1$ beam), is shown in the upper left panel of Fig. 3. While the strong local Galactic component peaks near 0 km s^{-1} , gas from the LLIV Arch shows its emission maximum at -57 km s^{-1} with $T_{\text{B}} \simeq 0.6 \text{ K}$, equivalent to a column density of $N(\text{HI}) = 3.45 \pm 0.09 \times 10^{19} \text{ cm}^{-2}$. This value agrees well with other HI emission line observations toward PG 0804+761 at lower angular resolution, such as obtained with the NRAO 140 ft (Murphy, Sembach & Lockman, in preparation; $21'$ beam) or the Leiden-Dwingeloo Survey (Hartman & Burton 1997; $36'$ beam). No HI emission is seen at velocities more negative than -100 km s^{-1} , where gas from Complex A is detected $< 0^{\circ}.5$ away (Wakker & van Woerden 1997).

The line of sight ends at the bright ($V = 15.2$) quasar PG 0804+761, in the literature cited to be at a redshift of $z_{\text{em}} = 0.100$ (Schmidt & Green 1983). Shull et al. (2000) reported absorption from an intervening Ly α absorber along this sight line at $+5565 \text{ km s}^{-1}$ or $z_{\text{abs}} = 0.019$, using HST STIS data. The latter component is also seen in Ly β absorption in the FUSE spectrum of PG 0804+761 (Shull et al. 2000). The

STIS data, however, do not cover the wavelength range above 1300 Å, so there is no information about intervening Ly α systems for redshifts $z > 0.069$. We will see in §5 that the FUSE data reveal one more intergalactic absorption component, which is most likely associated with PG 0804+761 itself.

3. Observations and Data Reduction

3.1. Observations

FUSE observations of PG 0804+761 were carried out on 1999 October 5 as one of the very first objects observed with FUSE. At this early state, FUSE had not reached its optimal performance so that this early data set was used only for a qualitative overview of the sight-line structure. Additional observations, with higher resolution and higher S/N, were performed in January 2000, using the large aperture (LWRS, $30'0 \times 30'0$) in the time-tag (TTAG) mode, in which the X and Y locations, the arrival time, and the pulse height of each detection are stored as a photon list. The quantitative analysis of the line of sight toward PG 0804+761 presented in the following sections relates to the data obtained in January. Basic information about these observations is given in Table 1. FUSE consists of four coaligned prime focus telescopes and Rowland-type spectrographs in combination with microchannel plate detectors. Two of the telescope channels have Al:LiF coatings, optimized for the wavelength range from 1000 to 1187 Å. The two other channels use SiC coatings and are sensitive from 905 to 1105 Å. More detailed descriptions of the instrument and its on-orbit performance are presented by Moos et al. (2000) and Sahnou et al. (2000). The spectral resolution of the PG 0804+761 data is $\lambda/\Delta\lambda \approx 12,000$, equivalent to 25 km s^{-1} , as estimated from profile fits for some of the weaker H₂ absorption lines. The average continuum flux in the spectrum is $\sim 8 \times 10^{-14} \text{ erg cm}^{-2} \text{ s}^{-1} \text{ Å}^{-1}$.

3.2. Data Reduction and Analysis Method

The total observing time for the spectrum of PG 0804+761 was 21,125 sec, recorded in five individual exposures (see Table 1). At the time that this paper was prepared, the absolute wavelength calibration for the early FUSE data was uncertain. We therefore measured the line centers for 20 absorption lines of molecular hydrogen in the local Galactic gas component and calibrated the wavelength scale by fixing the local H₂ gas component at $v_{\text{LSR}} \sim 0 \text{ km s}^{-1}$, representing the average of the two strong Galactic H I emission components around zero-velocities (Wakker et al. 2000). Wavelengths for the H₂ transitions are taken from the list of Abgrall & Roueff (1989); for atomic species we use the compilation of Morton (in preparation). From the internal scatter of the velocities for the H₂ line centers we estimate a mean accuracy of $\sim 10 \text{ km s}^{-1}$ for our wavelength calibration, but velocity deviations of more than 20 km s^{-1} still remain for some absorption lines in the spectrum. For these cases, the velocity scale was adjusted for each line individually with respect to the nearest reference line.

The data was extracted using the CALFUSE (Vers.1.6.6) standard reduction pipeline, providing the complete set of the individual exposures in each channel. The single exposures were coadded for each of the channels. In order to increase the signal- to-noise ratio (S/N), channels covering the same wavelength ranges were also combined. The latter procedure was made for each line individually, correcting for the deviations in the wavelength scale by adjusting the (Gaussian) line centers for the local Galactic component (at 0 km s^{-1}) to the zero point of the overall wavelength scale, as described above. We are aware of the fact that this combination introduces systematic errors in the flux distribution over the pixel scale. The increase of S/N,

however, justifies this procedure in view of the reduced uncertainty for the determination of absorption line equivalent widths. The spectra were rebinned over three pixels, but no additional smoothing was applied to the data. After combining and rebinning, the typical S/N turns out to be ~ 8 per (binned) pixel element. Fig. 2 shows part of the summary spectrum (all exposures, all channels) of PG 0804+761, plotted in flux units versus wavelength. The various interstellar absorption features have been marked and identified above the spectrum. Terrestrial emission features are also tagged. Fig. 3 shows a selection of continuum normalized interstellar absorption line profiles for PG 0804+761 plotted on a LSR velocity scale.

Equivalent widths W_λ have been measured by fitting multi-Gaussian components to observed line profiles. This method was chosen in view of the fact that the true line profiles from molecular hydrogen and weakly ionized species are not resolved in the FUSE data. For the O VI absorption, whose velocity profile is fully resolved at $\lambda/\Delta\lambda \approx 12,000$, we have measured W_λ by a direct pixel integration and its column density by making use of the apparent-optical-depth method, as described by Savage & Sembach (1991). Continua were normalized by fitting low-order polynomials to the data in the vicinity of each line. Errors for the W_λ , as given in Tables 2 and 4, include contributions from photon-counting statistics, from the fitting procedure, and from the continuum-placement errors.

4. Local Galactic Gas at 0 km s⁻¹

The spectrum of PG 0804+761 is dominated by absorption from molecular hydrogen and metals situated in the local Galactic ISM. Over 80 Galactic absorption lines are detected in the wavelength range between 920 and 1180 Å. Shull et al. (2000a) studied H₂ absorption in the Galactic gas component in the FUSE spectrum of PG 0804+761, finding a total H₂ column density of $N(\text{H}_2) = 6.1 \times 10^{18} \text{ cm}^{-2}$ and a temperature of $T_{0,1} = 113 \text{ K}$. In the present study, we do not discuss results for the local component. 74 Galactic absorption lines from neutral and molecular hydrogen and weakly ionized metals have been analyzed and their equivalent widths and errors can be made available by the authors. The metal lines detected include: C II ($\lambda 1036.337$), C III ($\lambda 977.020$), N I ($\lambda 953.415$, $\lambda 1134.980$), N II ($\lambda 1083.990$), O I ($\lambda 936.630$, $\lambda 971.738$), Si II ($\lambda 1020.699$), P II ($\lambda 1152.818$), Ar I ($\lambda 1048.220$, $\lambda 1066.660$), Fe II ($\lambda 1112.048$, $\lambda 1121.975$, $\lambda 1125.448$, $\lambda 1133.665$, $\lambda 1143.226$, $\lambda 1144.938$), and Fe III ($\lambda 1122.526$).

5. Absorption from Gas in the Lower Galactic Halo

The FUSE spectrum of PG 0804+761 shows absorption associated with the LLIV Arch at -55 km s^{-1} from the lowest two rotational states of molecular hydrogen, from various atomic species (C, N, O, Si, P, Ar, Fe), and from the Lyman series of neutral hydrogen.

5.1. Molecular Hydrogen

Weak absorption by molecular hydrogen (H₂) near -55 km s^{-1} associated with gas in the LLIV Arch is seen in several lines from the lowest 2 rotational states ($J = 0$ and 1). H₂ absorption profiles for six lines are presented in Fig. 3 in the left and middle panels. Equivalent widths for the detected absorption features range between 10 and 50 mÅ for lines with $\lambda \geq 980 \text{ Å}$. For the strongest of the H₂ transitions in the wavelength range below 980 Å, an accurate determination of the H₂ line strengths was not possible because

of the low signal-to-noise ratio in the two SiC channels and because of blending with Galactic H₂ absorption or atomic absorption lines. For $\lambda \geq 980 \text{ \AA}$ we measured equivalent widths for 5 lines and determined upper limits for 7 additional lines, as listed in Table 2. To derive column densities for the individual rotational states of H₂ we fitted the measurements to a curve of growth with $b = 6 \text{ km s}^{-1}$ (Fig. 4). This b -value represents the best fit to the observations. Its uncertainty ($\approx \pm 1 \text{ km s}^{-1}$) has only a minor influence on the determination of the column densities, since most of the lines are on the linear part of the curve of growth for which the choice of the b -value is unimportant. We obtained the H₂ column densities N for $J = 0$ and 1 and upper limits for the levels $J = 2, 3$, presented in Table 3. The errors for N are based on the uncertainties for the individual equivalent widths, the error of b , as well as the error for the fit to the curve of growth. Summing over the individual column densities for $J = 0, 1$ we find a total logarithmic H₂ column density of $\log N = 14.71 \pm 0.30$ for the gas in the LLIV Arch. The error here includes the upper limits in N for possible contributions from $J = 2, 3$. Together with $N(\text{H I}) = 3.45 \times 10^{19} \text{ cm}^{-2}$ from the Effelsberg 21 cm data, the fraction of hydrogen in molecular form is $f = 2N(\text{H}_2)/[N(\text{H I}) + 2N(\text{H}_2)] = 2.97 \times 10^{-5}$, a value which is similar to fractions found in local Galactic disk gas in sight lines with low interstellar reddening (Savage et al. 1977). The value indicates that the observed cloud is predominantly atomic. From the column densities of $J = 0$ and 1 we find an excitation temperature of $T_{0,1} = 193_{-75}^{+322} \text{ K}$ by fitting the level populations to a theoretical Boltzmann distribution.

The detection of molecular hydrogen in the LLIV Arch gives important information about the physical conditions in the intermediate-velocity gas in the lower Galactic halo. First, its presence shows that dust is present, since the efficient formation of H₂ requires dust grains as catalytic reaction partners (e.g., Pirronello et al. 1999). We shall see in the next section that this conclusion is in agreement with the actual metal abundance and depletion pattern in the LLIV Arch, as derived by the analysis of the metal lines in the FUSE spectrum. Second, the H₂ excitation temperature ($T_{0,1} = 193_{-75}^{+322} \text{ K}$) seems to be below the temperature expected directly after molecule formation ($\sim 300 \text{ K}$; e.g., Burton, Hollenbach & Tielens 1992), indicating that the H₂ gas has been thermalized to a temperature of 193 K. Thus, the excitation temperature might represent the kinetic temperature in the H₂ gas, suggesting the existence of cool (predominantly atomic) gas clumps in the LLIV Arch. However, in view of the large uncertainties for $T_{0,1}$ and the possibility, that the excitation is caused by thermalization processes on the grain surface, the causal connection between the excitation of the H₂ gas and the kinetic gas temperature remains speculative.

Molecular hydrogen in intermediate-velocity gas has also been detected toward HD 93521 (Gringel et al. 2000) and toward the LMC (de Boer 2000, priv. comm.). Though the molecular fractions are generally low, these results underline that the conditions in the lower Galactic halo allow molecular hydrogen and dust to exist, an aspect which certainly has to be considered for theoretical models of the Milky Way halo.

5.2. Neutral and Weakly Ionized Metals

Absorption at -55 km s^{-1} in low and intermediate ionization states of heavy elements is seen in the absorption profiles of C II, N I, N II, O I, Si II, P II, Ar I, Fe II and Fe III. Higher ionization states for these elements, such as C III and O VI, also clearly show absorption extended to negative velocities, but no separation between different velocity components can be made with the present data. Absorption from these higher ions will be discussed in §6. Fig. 3 presents normalized absorption profiles for some of the analyzed lines. The absorption pattern in metals is similar to that seen in neutral hydrogen emission (upper left panel of Fig. 3) and molecular hydrogen absorption. Equivalent widths, W_λ , for 18 lines at -55 km s^{-1} and their errors are given in Table 4. Typical relative errors for the equivalent widths are less than 20 percent. A

set of four Fe II lines accurately defines a curve of growth with $b = 8.0 \pm 0.7 \text{ km s}^{-1}$ (Fig. 4). This rather high value for b suggests that the velocity dispersion is primarily determined by non-thermal motions rather than by the true thermal widths of the lines. The fact that the b -value is higher for the ions than for the molecular hydrogen (see previous section) suggests that the weakly ionized material is more extended than the molecular gas, the latter most likely being situated in one or several confined regions. Column densities for the species listed above were determined by fitting the data values of $\log(W_\lambda/\lambda)$ to the curve of growth with $b = 8 \text{ km s}^{-1}$. The results are listed in Table 5. The column density errors include uncertainties from the individual errors of W_λ , the error in b , as derived from the dispersion of the Fe II data points, and the uncertainty for the fit to the curve of growth.

5.2.1. Ionization Effects

The presence of absorption by N II and Fe III at -55 km s^{-1} implies that a significant fraction of the hydrogen is ionized. We derive values of -0.86 for $\log(N(\text{N II})/N(\text{N I}))$ and -1.41 for $\log(N(\text{Fe III})/N(\text{Fe II}))$. This suggests that an ionization correction is required to determine accurate gas phase abundances in the gas of the LLIV Arch.

One can estimate the fraction of ionized hydrogen by comparing the relative abundances of P II and O I, assuming that the observed ionization states arise in the same physical region (i.e., in the same IVC). Ionization of O should be the same as for H, since both elements have a similar ionization potential and they are strongly coupled through charge exchange reactions. Phosphorus is not depleted in dust grains (Jenkins, Savage & Spitzer 1986) and the ionization potential of P II is 19.73 eV. We expect P II to be the dominant ionization state for phosphorus, and P II will exist where H and O are ionized. If we assume that $N(\text{P})/N(\text{O})_{\text{LLIV Arch}} \approx N(\text{P})/N(\text{O})_{\text{solar}}$ we can derive the ionization of O (and thus of H) by scaling the observed $(N(\text{P II})/N(\text{O I}))$ ratio in the LLIV Arch to the expected solar ratio. For the LLIV Arch we find $\log(N(\text{P II})/N(\text{O I})) = -3.21$, from which we estimate a degree of ionization $\text{H}^+ / (\text{H}^0 + \text{H}^+)$ of ~ 19 percent. This value fits well to the ionization fraction of N II ($\text{N}^+ / (\text{N}^0 + \text{N}^+) = 0.12$), which should roughly scale with the hydrogen photoionization fraction (Jenkins et al. 2000) and thus is an independent measure for the fraction of ionized hydrogen. In the following section, we will use the value of $\text{H}^+ / (\text{H}^0 + \text{H}^+) = 0.19$ for the determination of gas-phase abundances in the LLIV Arch.

5.2.2. Gas-Phase Abundances

For the analysis of gas phase abundances we use the compilation of solar reference abundances by Anders & Grevesse (1989), which are primarily based on meteoric data, except for C, N, and O, for which abundances from solar photosphere data were adopted (Grevesse & Noels 1993). For the H I column density in the LLIV Arch we take the value of $3.45 \pm 0.09 \times 10^{19} \text{ cm}^{-2}$ from the Effelsberg data. Taking into account the ionization fraction (see previous section), the total hydrogen column density is $N(\text{H}) = N(\text{H I}) + N(\text{H II}) = 4.26 \times 10^{19} \text{ cm}^{-2}$. The amount of hydrogen in molecular form (§5.1) does not contribute significantly to the total hydrogen column density.

The abundance pattern for the LLIV Arch along our sight line (Table 6, Fig. 5) is similar to that for diffuse warm clouds in the disk of the Milky Way (Savage & Sembach 1996). Because of the reasons described in the previous section, the O I/H I ratio should be representative of the actual oxygen abundance in the gas and thus provide a good measure for the overall metallicity. We find $\log(N(\text{O I})/N(\text{H I})) = -3.12 \pm 0.23$,

which is $1.03^{+0.71}_{-0.42}$ solar. Note that there are additional systematic uncertainties in this and the other element abundances due to the fact that we compare UV absorption line data with beam smeared H I emission line measurements. Another problem is that the absorption lines for O I as well as the ones from N I are saturated and are located on the intermediate part of the curve of growth where small errors for W_λ cause large uncertainties in the determination of the column densities. Thus, the column densities for N I, N II and O I are most uncertain, while the equivalent widths of their lines have the smallest relative errors (see error bars in Fig. 5). The relatively low abundance of N ($=N_{\text{I}}+N_{\text{II}}$) in comparison to O I and P II (see Fig. 5) might be a result of the uncertainty of $N(\text{N I})$ derived with the curve-of-growth technique. We also note that an additional systematic uncertainty may arise from the errors for the oscillator strengths f . Within the error bars, however, a nearly solar gas phase abundance of the LLIV Arch is consistent with the individual abundances of N, O, and P.

In contrast to N, O I, and P II, the normalized logarithmic gas-phase abundances of Fe II and Si II are ≤ -0.40 dex (Fig. 5), most likely as a result of depletion into dust grains. Such depletion is consistent with the detection of H₂ in the LLIV Arch (see §5.1), which is an independent tracer for the presence of dust in this component. The strong deficiency of Ar I ($[\text{Ar I}/\text{H I}] = -0.68 \pm 0.07$) is most likely due to an over-ionization of Ar I. Sofia & Jenkins (1998) argued that a deficiency in the Ar I abundance can be explained by its very large photoionization cross section. They find that the Ar I/H I ratio is lowered in a range between -0.11 and -0.96 dex in regions that are significantly ionized, which is in agreement with our measurements. In principle, one might verify this result by inspecting the Ar II line at 919.781 Å, but the low oscillator strength and the low S/N at these wavelengths make this line undetectable in our spectrum.

The nearly solar gas-phase abundances for O, N and P in combination with the presence of molecules and dust strongly indicates that the gas in the LLIV Arch has its origin in the Galactic disk. We therefore conclude that the LLIV Arch is most likely part of the return flow of a Galactic fountain (Shapiro & Field 1976; Houck & Bregman 1990) or other mechanism that links star formation in the disk to the interstellar material in the lower Galactic halo.

6. Moderately and Highly Ionized Gas

In addition to the absorption lines of molecular hydrogen and weakly ionized metals, the FUV range gives access to information about moderately and highly ionized gas through the strong absorption lines of C III at 977.020 Å and the O VI doublet at 1031.926 and 1037.617 Å. The ionization energy of C III is 47.89 eV; thus C III traces moderately ionized gas at temperatures of $\sim 10^4$ K. The C III line has a large oscillator strength ($f = 0.762$) and becomes quickly saturated because of the high abundance of carbon in the ISM. Strong absorption from intermediate ionization states from other species (e.g., Si III and Si IV) has been found in sight lines to extragalactic background sources using STIS and GHRS data (Savage, Sembach & Lu 1997; Fabian et al., in preparation), suggesting that moderately ionized gas is a dominant constituent in the lower Galactic halo. Unfortunately, the C III absorption at negative velocities is blended by the absorption profile of the O I line at $\lambda = 976.448$ Å (see Fig. 3), thus making an analysis of the velocity distribution of C III toward PG 0804+761 impractical.

From the two O VI absorption lines in the spectrum of PG 0804+761 only the one at 1031.926 Å is unblended and can be used to study the highly ionized gas ($T \simeq 3 \times 10^5$ K) in direction of PG 0804+761. Savage et al. (2000) included the early PG 0804+761 observations in their determination of a O VI scale height of the Milky Way halo. Using data from the observations performed in November, they found an

equivalent width of $286 \pm 19 \text{ m}\text{\AA}$ for the O VI line at 1031.926 \AA and derived from that a column density of $\log N(\text{O VI}) = 14.50 \pm 0.04$. With the new data set from the observations in January we find $W_\lambda = 260 \pm 17 \text{ m}\text{\AA}$ and $\log N(\text{O VI}) = 14.38 \pm 0.06$, integrating the O VI absorption profile in the range between -150 to $+100 \text{ km s}^{-1}$. The O VI $\lambda 1031.926$ line profile is presented in Fig. 3. Interestingly, it shows O VI absorption extended to velocities as negative as -110 km s^{-1} . In general, O VI absorption around zero velocities is thought to trace the thick O VI halo of the Milky Way and is seen in many extragalactic sightlines in different directions (Savage et al. 2000). High velocity O VI ($|v_{\text{LSR}}| > 100 \text{ km s}^{-1}$) is seen in several extended sight lines toward AGNs and quasars (Sembach et al. 2000). These velocities lie beyond the integration range expected for O VI absorption in the environment of the thick disk and the lower Galactic halo. In all cases, high velocity O VI absorption can be related to high-velocity clouds or known structures in the outer Galaxy (see Sembach et al. 2000).

For the sight-line toward PG 0804+761 there are different possible explanations for the O VI absorption extending to -110 km s^{-1} :

- (1) The extended O VI absorption might be due to a hot gas layer surrounding Complex A. While one might expect that Complex A has a gaseous envelope containing highly ionized species so close to its H I boundaries, we reject this possibility because H I gas from Complex A close to our sight line is seen at -180 km s^{-1} (Wakker & van Woerden 1997), which is a radial velocity 70 km s^{-1} more negative than the O VI absorption.
- (2) The extended O VI absorption along the sight line might represent highly ionized gas related to the envelope of the LLIV Arch. If there is a dynamical interaction between the cooler intermediate-velocity gas and a hot surrounding medium one might expect that the radial velocities for the O VI absorption should correspond to the radial velocity of the weakly ionized gas. Since thermal and turbulent broadening would smear the O VI absorption profile as far as the observed -110 km s^{-1} , the observed profile is consistent with O VI absorption in the LLIV Arch.
- (3) The extended O VI absorption might be related to hot gas above the Perseus arm. Savage, Sembach & Lu (1995) found C IV absorption at -70 km s^{-1} toward H1821+643 ($l = 94^\circ 0, b = 27^\circ 4$) and concluded that this component is related to hot gas situated 1.5 kpc above the Perseus arm. FUSE observations of H 1821+643 (Oegerle et al. 2000) have also revealed O VI absorption that is likely associated with the Perseus arm. Several arguments favor a similar explanation for the extended O VI absorption toward PG 0804+761: First, the sight line toward PG 0804+761 passes the Perseus arm exactly above a region where a Galactic chimney has been found, driven by the open cluster OC1352 in the Cassiopeia OB6 association region at $l = 134^\circ 8, b = 0^\circ 9$ (Normandeau, Taylor & Dewdney 1996). If chimneys such as this are common features in the active regions in the Milky Way’s spiral arms, they should contribute significantly to the mass transfer of hot gas into the Galactic halo (Shapiro & Benjamin 1991; Norman & Ikeuchi 1989) and would explain the presence of hot gas above the Perseus arm and other active regions. Second, due to Galactic rotation, gas associated with the Perseus arm in this direction is seen at velocities around -50 km s^{-1} (Kepner 1970), consistent with the observed O VI absorption extended to negative velocities when the effects of line broadening and instrumental blurring are included.

Although we favor (3) for explaining the observed O VI absorption profile toward PG 0804+761, we cannot exclude that high-velocity O VI absorption is due to a highly ionized boundary of the LLIV Arch (2), or a combination of both possible contributors.

7. Complex A

Considering that PG 0804+761 falls just outside the known neutral edge of Complex A (see Fig. 1), we might expect to see absorption associated with an ionized shell around Complex A. No clear H I absorption is seen in the higher Lyman lines at Complex A velocities ($\sim -180 \text{ km s}^{-1}$), thus ruling out a low density neutral envelope around Complex A down to a 3σ level of $\log N(\text{H I}) < 14.84$. Unfortunately, the most sensitive tracer for moderately ionized gas, the C III line at 977.020 \AA , is blended by Galactic O I absorption (see previous section). The N III line at 989.799 \AA is not strong enough to obtain useful information about its abundance at the given S/N in that wavelength region. O VI absorption extends to velocities of $\sim -110 \text{ km s}^{-1}$, but not beyond (see previous section). We conclude that no meaningful information about abundances in Complex A is yielded by the FUSE data of PG 0804+761. However, the observations do imply that the boundary of Complex A in this direction contains very little H I, and O VI, thus indicating that Complex A has a well defined, sharp edge in this direction.

8. Intergalactic Gas

Six features in the spectrum can not be associated with lines from gas in the inner or outer Milky Way, but have been identified as intergalactic absorption lines. They are listed in Table 7.

8.1. Intervening Absorption at $z = 0.019$

Shull et al. (2000b) identified weak Ly β absorption at $+5565 \text{ km s}^{-1}$ ($z = 0.019$) in the early FUSE spectrum of PG 0804+761 in a FUSE mini-survey on intergalactic Ly β absorbers at low redshifts. At this velocity, absorption by Ly α was previously detected in the STIS spectrum of PG 0804+761 (see Shull et al. 2000b). They give a restframe equivalent width of $W_\lambda = 90 \pm 30 \text{ m\AA}$ for the Ly β line, based on the early FUSE data from November 1999. With the new data, we find Ly β absorption at 1044.710 \AA (equivalent to $+5553 \text{ km s}^{-1}$ or $z = 0.0185 \pm 0.0004$) and $W_\lambda(\text{rest}) = 73 \pm 22 \text{ m\AA}$, in agreement with the earlier results. No O VI absorption is seen at $z = 0.0185$. 3σ upper limits for restframe equivalent widths of the two O VI absorption lines at $\lambda_{\text{rest}} = 1031.926$ and 1037.617 \AA are 64 and 52 m\AA , respectively.

8.2. The Associated System at $z = 0.102$

The strongest intergalactic absorption component is found at $z = 0.102$. This feature is most likely related to the quasar PG 0804+761 itself (an “associated system” or “intrinsic absorber”). This absorber is not seen in the HST data since the wavelength coverage of the STIS spectrum does not extend above 1300 \AA , equivalent to a limiting redshift of $z = 0.069$ for the Ly α line. The associated system is seen in neutral hydrogen (Ly β , Ly γ) as well as in moderately (C III) to highly (O VI) ionized species. Normalized line profile plots on a $z_{\text{abs}} = 0.102$ restframe velocity scale for the detected lines (except C III which is blended by Galactic H₂ R(0),2-0) are presented in Fig. 6. Restframe equivalent widths and column densities are given in Table 7. Based on the uncertainty of the wavelength calibration, we estimate an uncertainty for the redshift seen in absorption of $\sigma(z) \approx 0.0004$.

Interestingly, we see the associated system at $z_{\text{abs}} = 0.102$, while PG 0804+761 is cited in the literature to be at $z_{\text{em}} = 0.100$, based on the Bright Quasar Survey from Schmidt & Green (1983), a subsample of the

Palomar-Green Survey (Green, Schmidt & Liebert 1986). Their redshift is based on the measurement of two O III emission lines at redshifted wavelengths of $\lambda 5453$ and $\lambda 5507$ at a resolution of 10 \AA (Green, Schmidt & Liebert 1986). The redshift displacement between their emission line measurements and our absorption line analysis (at $\sim 0.1 \text{ \AA}$ resolution) is $\Delta z = 0.002$, which is similar to one resolution bin in their data and thus roughly representative of the uncertainty in their cited redshifts. From the estimated error of $\sigma(z) \approx 0.0004$ in the FUSE data, it is therefore probable that the actual redshift of PG 0804+761 is $z = 0.102$ rather than $z = 0.100$. It cannot be excluded, however, that the offset between z_{em} and z_{abs} is real and thus reflects the intrinsic motion of the absorber with respect to the quasar.

The associated absorber clearly shows substructure in its line profiles, seen in H I as well as in the stronger one of the two O VI lines (see Fig. 6). We identify at least two components, the stronger one at a restframe velocity of 0 km s^{-1} , and a weaker component near -45 km s^{-1} . More absorption components might be present but are not resolved in the FUSE data. The absorption in the associated system could be due to gas in and/or around the host galaxy of PG 0804+761 itself. Another possibility is that this gas is related to neutral and highly ionized gas in a different system in front of PG 0804+761, possibly located in a galaxy cluster together with PG 0804+761. The logarithmic column densities of H I and O VI are ~ 14.3 and ~ 14.0 , respectively (see Table 7). They are close to values found for intervening O VI absorbers, such as the system at $z = 0.142$ toward PG 0953+415 (Tripp & Savage 2000). It is not clear whether low redshift associated and intervening systems share the same physical conditions. While collisional ionization is favoured for the intervening O VI absorber toward PG 0953+415 (Tripp & Savage 2000), the associated system toward PG 0804+761 could also be photoionized by the quasar itself or other surrounding photon sources in combination with the overall EUV background field. Additional absorption line measurements with higher resolution in combination with optical data are required to study structure, abundances and ionization conditions in the associated system toward PG 0804+761 in more detail.

8.3. Intervening O VI Systems

In the following, we briefly discuss the fact that we do not find any intervening O VI absorption systems along a sight line with a redshift path of 0.102 and its implications for the estimate of the number density per unit redshift of intergalactic O VI absorbers, recently discussed in the work by Tripp, Savage & Jenkins (2000). These authors give a value of $dN/dz > 17$ for absorption with $W_\lambda \geq 30 \text{ m\AA}$ at a 90 percent confidence level for these reservoirs of hot baryonic matter in intergalactic space, based on HST STIS data toward the quasar H1821+643 ($z = 0.297$). While the redshift of PG 0804+761 is 0.102, the actual redshift range which can be investigated for O VI absorbers is much smaller due to blending with the various ISM absorption features. We separate intervening from associated systems at a velocity of 6000 km s^{-1} away from the quasar, corresponding to a limiting wavelength of 1121 \AA . All identified ISM absorption features in the spectrum between 1032 and 1121 \AA obscure $\sim 16.5 \text{ \AA}$, as measured by integrating their individual blocking in the spectrum. Since we require the detection of *both* lines of the O VI doublet to provide a definite detection, the effective blockage is $\sim 33 \text{ \AA}$ of a total of 89 \AA . Thus, the redshift path in the spectrum of PG 0804+761 suitable to investigate intervening O VI systems is reduced from 0.102 to 0.054. Assuming that $dN/dz \approx 17$ for these systems with $W_\lambda \geq 30 \text{ m\AA}$, one would expect one intervening O VI system toward PG 0804+761. The average detection limit in the FUSE spectrum of PG 0804+761, however, is $\sim 50 \text{ m\AA}$, so that the expected number of O VI systems visible in the FUSE spectrum will be substantially smaller than one. Therefore, the non-detection of intervening O VI systems in this data set is consistent with expectations based on the small unobscured redshift path and the relatively large limiting equivalent width.

9. Summary

We present FUSE far ultraviolet observations at intermediate resolution of interstellar and intergalactic absorption lines along the line of sight toward the quasar PG 0804+761 at $z_{\text{abs}} = 0.102$. Along this sight line we find absorption from molecules and weakly ionized species in local Galactic gas at 0 km s^{-1} , and in gas associated with the Low Latitude Intermediate Velocity Arch (LLIV Arch) in the lower Galactic halo at -55 km s^{-1} . We also detect absorption from highly ionized gas in the Galactic halo extended to velocities as negative as -110 km s^{-1} , and from intergalactic gas at redshifts of $z = 0.019$ and 0.102 , the latter most likely being associated with the quasar itself.

1. We find H_2 absorption in gas of the LLIV Arch with a total column density of $\log N = 14.71 \pm 0.3$ from the lowest 2 rotational states ($J = 0$ and 1). An excitation temperature of 193_{-75}^{+322} K is derived for the H_2 gas from a Boltzmann fit to the relative populations of the rotational states $J = 0, 1$. From the presence of H_2 in the LLIV Arch we conclude that dust is present in this cloud in the lower Galactic halo.

2. An analysis of metal abundances in the LLIV Arch is performed, including absorption lines from C II, N I, N II, O I, Si II, P II, Ar I, Fe II and Fe III. For O I, we find a gas phase abundance of $1.03_{-0.42}^{+0.71}$ solar. The presence of N II and Fe III indicates that a substantial fraction of the gas is ionized. We estimate a degree of ionization of $\text{H}^+ / (\text{H}^0 + \text{H}^+) \approx 0.19$. The presence of dust, molecules and metals at nearly solar abundances lead us to conclude that the LLIV Arch is part of the return flow of a Galactic fountain.

3. We investigate velocity profiles of the moderately and highly ionized species C III and O VI. While C III absorption is blended by an O I line, we find O VI absorption at $\lambda = 1031.926 \text{ \AA}$ extended to negative velocities as far as -110 km s^{-1} . We suggest that the O VI absorption at these negative velocities is related to highly ionized gas situated above the Perseus spiral arm. Another possibility is that the O VI absorption is due to a highly ionized envelope of the LLIV Arch.

4. Six intergalactic absorption lines of H I, C III and O VI are found at redshifts of $z = 0.019$ and 0.102 . The latter absorber is probably associated with the quasar PG 0804+761 itself. The non-detection of intervening O VI absorbers adds information about the number density per unit redshift of intergalactic O VI absorbers at low redshift.

We thank the FUSE Science and Operations Teams for their dedicated efforts to make the observations described in this paper possible. We also thank Todd M. Tripp for helpful comments on the IGM part of this study. This work is based on data obtained for the the Guaranteed Time Team by the NASA-CNES-CSA FUSE mission operated by the Johns Hopkins University. Financial support has been provided by NASA contract NAS5-32985.

REFERENCES

- Abgrall, H., Roueff, E. 1989, *A&AS*, 79, 313
- Anders, E., Grevesse, N. 1989, *Geochim. Cosmochim. Acta* 53, 197
- Burton, M.G., Hollenbach, D.J., Tielens, A.G.G.M. 1992, *ApJ*, 399, 563
- de Boer, K.S., Rodriguez Pascual, P., Wamsteker, W., Sonneborn, G., Fransson, C., Bomans, D.J., Kirshner, R.P. 1993, *A&A*, 280, L15

- de Boer, K.S., Richter, P., Bomans, D.J., Heithausen, A., Koornneef, J. 1998, *A&A*, 338, L5
- Green, R.F., Schmidt, M., Liebert, J. 1986, *ApJS*, 61, 305
- Grevesse, N., & Noels, A. 1993, in *Origin of the Elements*, ed. N. Prantzos, E. Vangioni-Flam, & M. Cassé, (Cambridge: Univ. Press), 15
- Gringel, W., Barnstedt, J., de Boer, K.S., Grewing, M., Kappelman, N., Richter, P. 2000, *A&A*, 358, L37
- Houck, J.C., Bregman, J.N. 1990, *ApJ*, 352, 506
- Hartmann, D., Burton, W.B. 1997, *Atlas of Galactic Neutral Hydrogen*, Cambridge University Press
- Hulsbosch, A.N.M., Wakker, B.P. 1988, *A&AS*, 75, 191
- Jenkins, E.B., Savage, B.D. & Spitzer L. 1986, *ApJ*, 301, 355
- Jenkins, E.B., et al. 2000, *ApJ*, 538, L81
- Kepner, M. 1970, *A&A*, 5, 444
- Kuntz, K.D., Danly, L. 1996, *ApJ*, 457, 703
- Moos, H.W., et al. 2000, *ApJ*, 538, L1
- Norman, C.A., & Ikeuchi, S. 1989, *ApJ*, 345, 372
- Normandeau, M., Taylor, A.R., Dewdney, P.E. 1996, *Nature*, 380, 687
- Oegerle, W.R., et al. 2000, *ApJ*, 538, L23
- Pirronello V., Liu, C., Roser, J.E., Vidali, G. 1999, *A&A*, 344, 681
- Reynolds, R.J., Tuftte, S.L., Kung, D.T., McCullough, P.R., Heiles, C. 1995, *ApJ*, 448, 715
- Ryans, R.S.I., Keenan, F.P., Sembach, K.R., Davies, R.D. 1997, *MNRAS*, 289, 986
- Richter, P., et al. 1998, *A&A*, 338, L9
- Richter, P., de Boer, K.S., Widmann, H., Kappelman, N., Gringel, W., Grewing, M., Barnstedt, J. 1999
Nature, 403, 386
- Sahnow, D.J., et al. 2000, *ApJ*, 538, L7
- Savage, B.D., Drake, J.F., Budich, W., Bohlin, R.C. 1977, *ApJ*, 216, 291
- Savage, B.D., Sembach, K.R. 1991, *ApJ*, 379, 245
- Savage, B.D., Sembach, K.R., Lu, L. 1995, *ApJ*, 449, 145
- Savage, B.D., Sembach, K.R. 1996, *ARA&A*, 34, 279
- Savage, B.D., Sembach K. R., Lu, L. 1997, *AJ*, 113, 2158
- Savage, B.D., et al. 2000, *ApJ*, 538, 27
- Schmidt, M., Green, R.F. 1983, *ApJ*, 269, 352

- Sembach, K.R., et al. 2000, ApJ, 538, L31
- Shapiro, P.R., & Field, G.B. 1976, ApJ, 205, 762
- Shapiro, P.R., Benjamin, R.A 1991, PASP, 103, 923
- Shull, J.M., et al. 2000a, ApJ, 538, L73
- Shull, J.M., et al. 2000b, ApJ, 538, L16
- Sofia, U.J., & Jenkins, E.B. 1998, ApJ, 499, 951
- Snow, T.P., et al. 2000, ApJ, 538, L65
- Spitzer, L., & Jenkins, E.B. 1975, ARA&A, 13, 133
- Tripp, T.M., & Savage, B.D. 2000, ApJ, in press (astro-ph/0004135)
- Tripp, T.M., Savage, B.D., Jenkins, B.D. 2000, ApJ, 534, L1
- Vladilo, G., Centurión, M., de Boer, K.S., King, D.L., Lipman, K., Stegert, J.S.W., Unger, S.W., Walton, N.A. 1993, A&A, 280, L11
- Vladilo, G., Centurión, M., de Boer, K.S., King, D.L., Lipman, K., Stegert, J.S.W., Unger, S.W., Walton, N.A. 1994, A&A, 291, 425
- Wakker, B.P., Howk, C., van Woerden, H., Schwarz, U.J., Beers, T.C., Wilhelm, R., Kalberla, P.M.W., Danly, L. 1996, ApJ, 473, 834
- Wakker, B.P., van Woerden H. 1997, ARA&A, 35, 217
- Wakker, B.P. 2000, ApJS, submitted
- Wakker, B.P., Kalberla, P.M.W., van Woerden, H., de Boer, K.S., Putman M.E. 2000, ApJS, submitted
- Welsh, B.Y., Craig, N., Roberts, B. 1996, A&A, 308, 428
- Widmann, H., et al. 1998, A&A, 338, L1

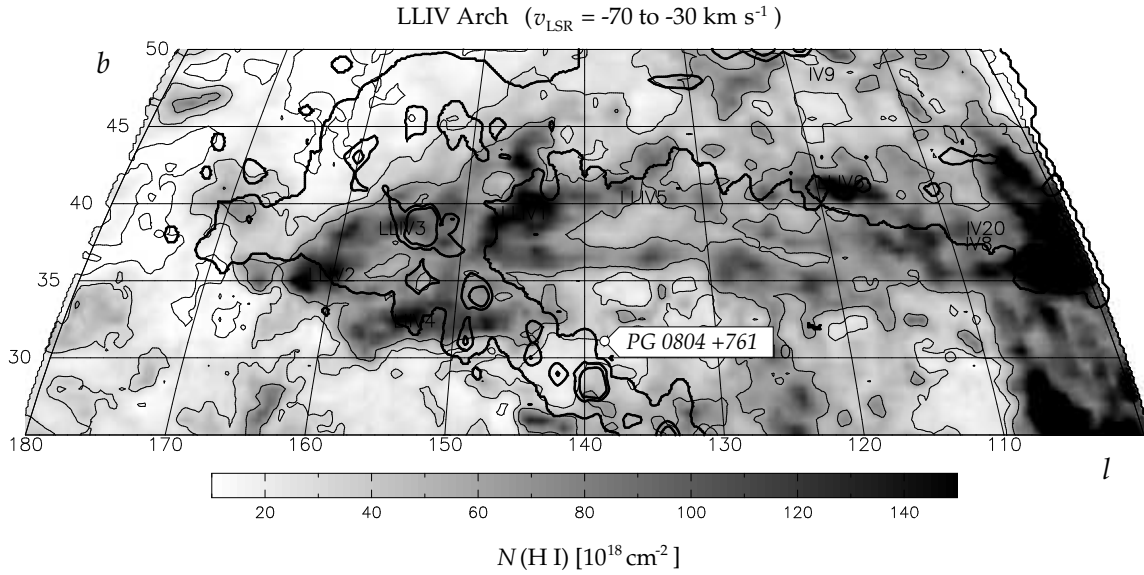


Fig. 1.— The greyscale and thin contours show the HI column density of the LLIV Arch (Kuntz & Danly 1996), in the velocity range between -70 and -30 km s^{-1} , from the Leiden-Dwingeloo Survey (Hartmann & Burton 1997). Contour levels are at $1, 4, 8$ and $16 \times 10^{19} \text{ cm}^{-2}$. The thick contours give brightness temperature levels of $0.05, 0.7$ and 1.2 K for the high-velocity gas ($v_{\text{LSR}} < -100 \text{ km s}^{-1}$) from the data of Hulsbosch & Wakker (1988). These approximately correspond to column densities of $0.25, 3$ and $5 \times 10^{19} \text{ cm}^{-2}$.

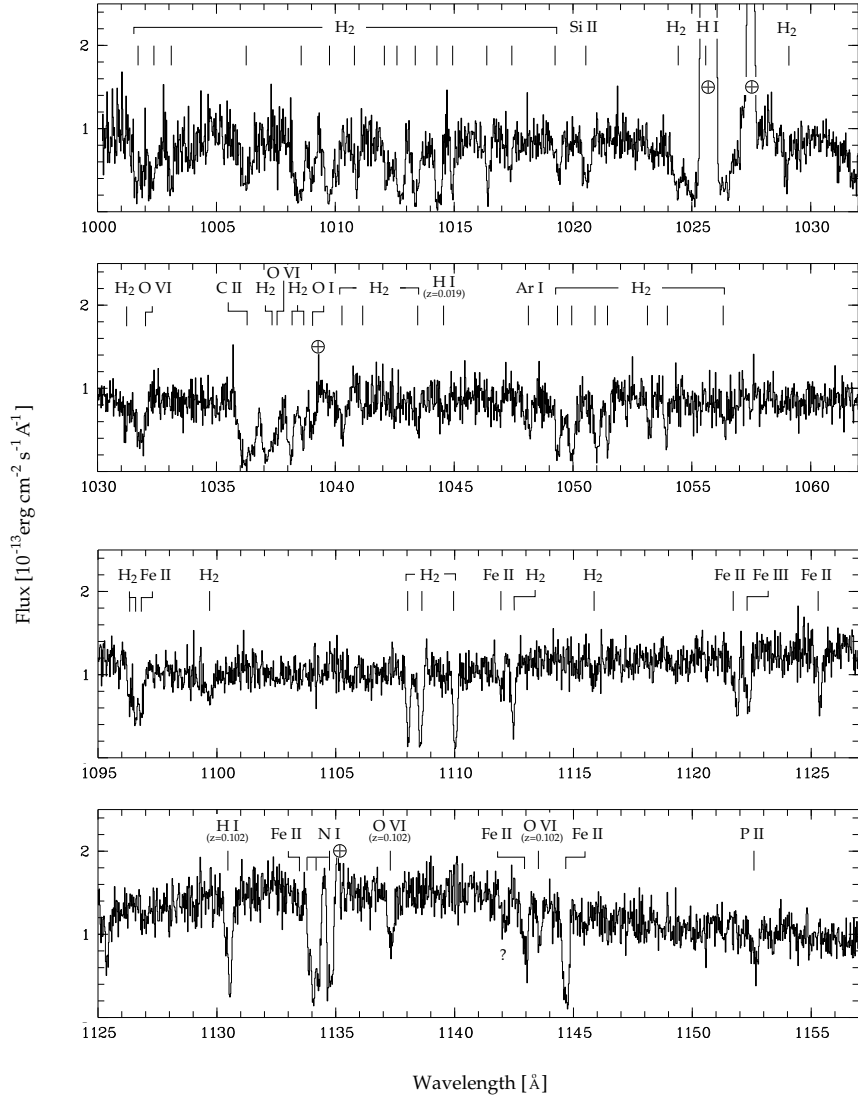


Fig. 2.— Portions of the FUSE spectrum of PG 0804+761 over the wavelength ranges from 1000 – 1062 Å and 1095 – 1157 Å are shown. The plotted data represent a summary spectrum combining all channels and their segments. The data has been binned over 3 pixels. Galactic molecular and atomic absorption lines (centered at their local Galactic component at $v_{\text{LSR}} = 0$ km s $^{-1}$) and intergalactic absorption features (presented together with their redshifts) are identified above the spectrum. Terrestrial emission features are marked with a \oplus .

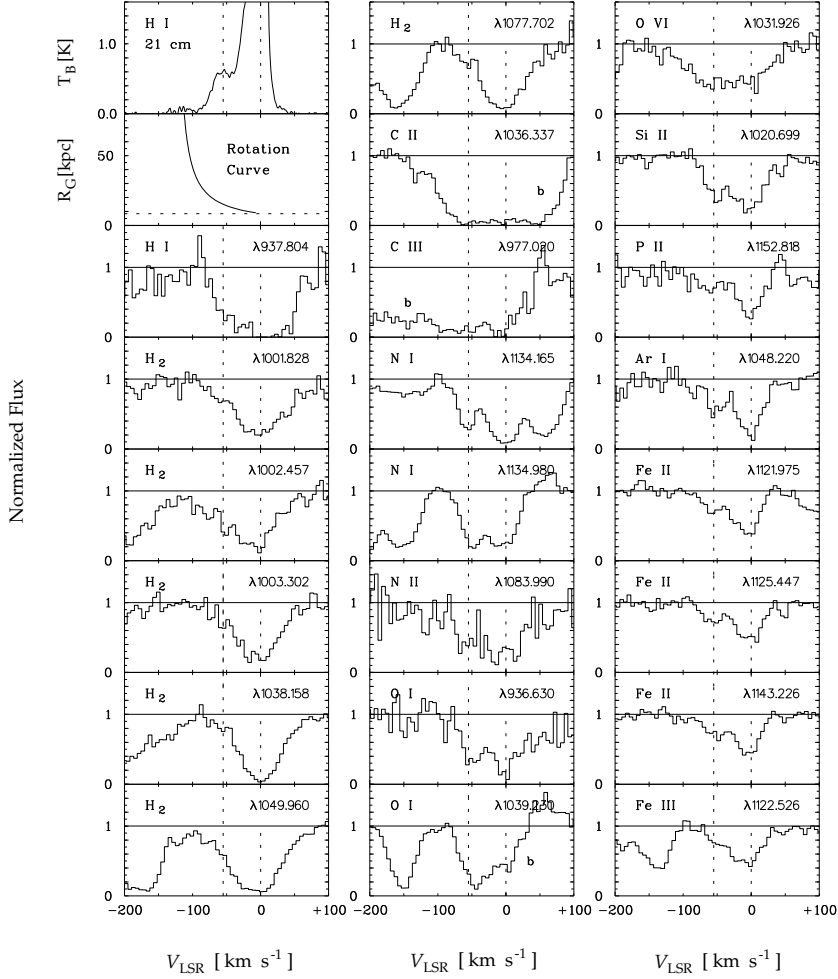


Fig. 3.— Continuum normalized interstellar absorption profiles for PG 0804+761 are plotted against LSR velocity. They include absorption from molecular hydrogen and atomic species at low and high ionization states. The individual profiles are labeled within each box. Local Galactic absorption is seen at 0 km s^{-1} ; absorption associated with the LLIV Arch appears at -55 km s^{-1} . Both velocities are marked with dotted lines. The O VI absorption line (upper right box) shows absorption at velocities as negative as -110 km s^{-1} . At the top of the left panel we show the Effelsberg H I 21 cm emission temperature profile (Wakker et al. 2000; 9/1 beam) and the relation between LSR velocity and Galactocentric distance, R_G , for co-rotating gas and a flat Galactic rotation curve with $\Theta(R_G \geq 8.5 \text{ kpc}) = 220 \text{ km s}^{-1}$. Regions blended by other lines are labeled with “b”.

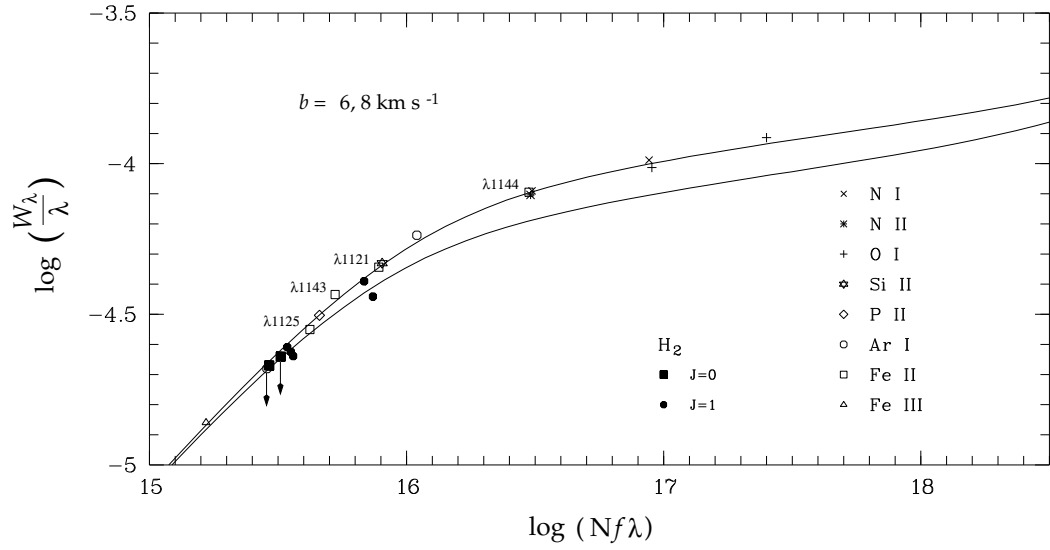


Fig. 4.— Empirical curves of growth for the ion states and molecular hydrogen levels detected in the LLIV Arch toward PG 0804+761. The ions collectively fit on a curve of growth with $b = 8 \text{ km s}^{-1}$, defined by four Fe II lines. The data points for these lines are shown together with their wavelengths. The molecular hydrogen lines from $J = 0$ and 1 fit on a curve of growth with $b = 6 \text{ km s}^{-1}$. The individual species are labeled in the lower right corner.

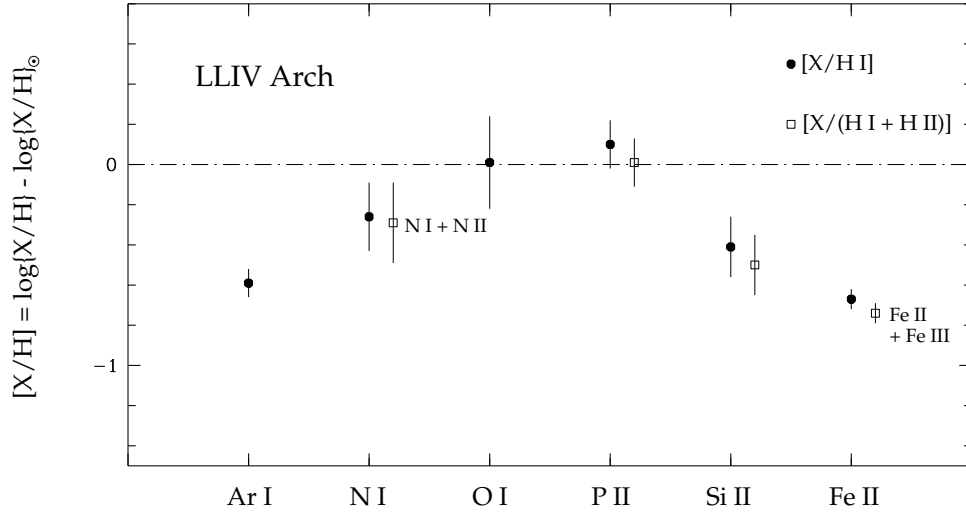


Fig. 5.— Normalized gas-phase abundances of several ionic species associated with gas in the LLIV Arch at -55 km s^{-1} . Gas phase abundances are referenced to H I (filled circles) and H I+H II (open squares); they are listed in Table 6. The elements are sorted by their condensation temperature (increasing from left to the right, see Savage & Sembach 1996).

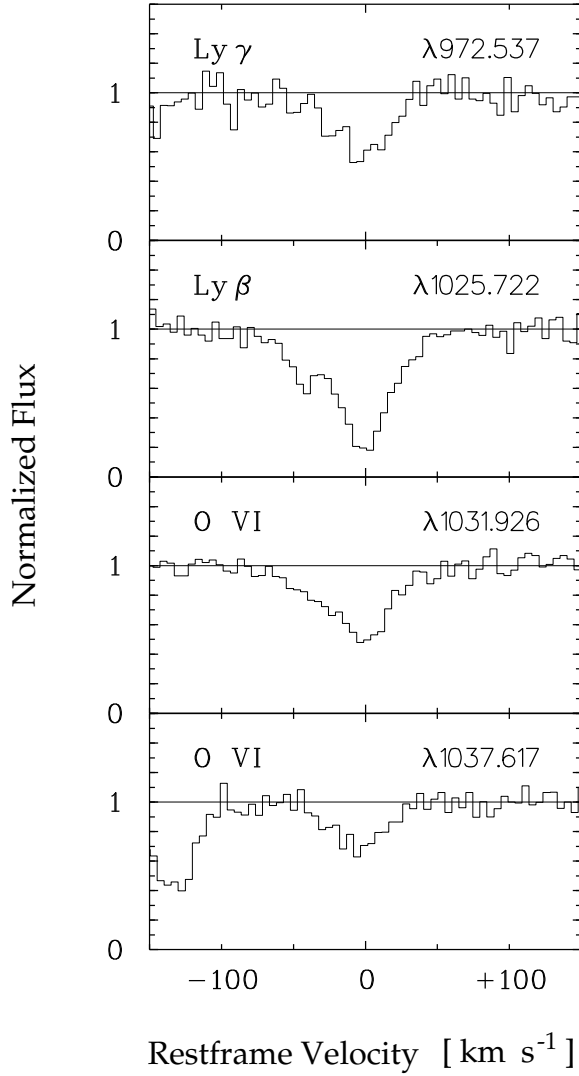


Fig. 6.— Velocity profiles for the absorbing system at $z_{\text{abs}} = 0.102$ associated with the background quasar PG0804+761. The velocity scale is referenced to the redshift of $z = 0.102$. The associated system is seen in H I, C III, and O VI and shows a two-component structure in the strong lines of H I $\lambda 1025.722$ and O VI $\lambda 1031.926$ with the main component at 0 km s^{-1} and a weaker component at $\sim -45 \text{ km s}^{-1}$. The profile for C III is not shown here because it is strongly blended by Galactic H₂ R(0),2-0 absorption.

Table 1. Log of FUSE Observations

Target Name	FUSE Dataset Name	Obs. Date	Exp. Time [sec]
PG 0804+761	P1011903001	Jan. 04 2000	3464 ^a
PG 0804+761	P1011903002	Jan. 04 2000	4730 ^a
PG 0804+761	P1011903003	Jan. 04 2000	4449
PG 0804+761	P1011903004	Jan. 04 2000	4291
PG 0804+761	P1011903005	Jan. 04 2000	4191

^aNo SiC 1 channel.

Table 2. H₂ Absorption Lines at the Velocity of the LLIV Arch^a

J	Transition	$\lambda_{\text{vac}}^{\text{b}}$ [Å]	$\log \lambda f^{\text{b}}$	W_{λ}^{c} [mÅ]	Channel
0	Lyman R(0),8-0	1001.828	1.432	21 ± 9	LiF 1A, LiF 2B
0	Lyman R(0),6-0	1024.376	1.473	≤ 42	LiF 1A, LiF 2B
1	Lyman R(1),8-0	1002.457	1.256	36 ± 9	LiF 1A, LiF 2B
1	Lyman P(1),8-0	1003.302	0.931	25 ± 8	LiF 1A, LiF 2B
1	Lyman P(1),5-0	1038.158	0.956	24 ± 6	LiF 1A, LiF 2B
1	Lyman R(1),4-0	1049.960	1.225	43 ± 6	LiF 1A, LiF 2B
1	Lyman R(1),2-0	1077.702	0.919	26 ± 7	LiF 1A
2	Werner Q(2),0-0	1010.941	1.381	≤ 15	LiF 1A, LiF 2B
2	Lyman P(2),5-0	1040.368	1.017	≤ 21	LiF 1A, LiF 2B
3	Lyman R(3),6-0	1028.988	1.243	≤ 28	LiF 1A, LiF 2B
3	Lyman P(3),5-0	1043.504	1.060	≤ 19	LiF 1A, LiF 2B
3	Lyman R(3),4-0	1053.975	1.137	≤ 29	LiF 1A, LiF 2B

^aEquivalent widths are reported for H₂ absorption at the velocity $v_{\text{LSR}} \approx -55 \text{ km s}^{-1}$ which associates the absorption with the LLIV Arch.

^bVacuum wavelengths and oscillator strengths from Abgrall & Roueff (1989).

^cEquivalent widths, 1σ errors, or upper limits are listed.

Table 3. H₂ Column Densities in the LLIV Arch

J	b [km s ⁻¹]	log N
0	6	14.04 ± 0.11
1	6	14.61 ± 0.13
2	6	≤ 14.33
3	6	≤ 14.36
Total		14.71 ± 0.30

Table 4. Atomic Absorption Lines in the LLIV Arch

Species	$\lambda_{\text{vac}}^{\text{a}}$ [Å]	$\log \lambda f^{\text{a}}$	W_{λ}^{b} [mÅ]	Channel
H I	937.804	0.864	$225 \pm 32^{\text{c}}$	SiC 1B, SiC 2A
C II . . .	1036.337	2.104	≤ 94	LiF 1A, LiF 2B
N I	953.415	1.098	≤ 80	SiC 2A
	1134.165	1.238	92 ± 6	LiF 1B, LiF 2A
	1134.980	1.693	117 ± 7	LiF 1B, LiF 2A
N II . . .	1083.990	2.097	85 ± 21	SiC 2B
O I	936.630	0.534	91 ± 18	SiC 2A
	1039.230	0.980	127 ± 30	LiF 1A, LiF 2B
Si II . . .	1020.699	1.225	48 ± 7	LiF 1A, LiF 2B
P II . . .	1152.818	2.451	36 ± 7	LiF 1B, LiF 2A
Ar I . . .	1048.220	2.440	61 ± 7	LiF 1A, LiF 2B
	1066.660	1.857	≤ 22	LiF 1A, LiF 2B
Fe II . . .	1121.975	1.512	51 ± 5	LiF 1B, LiF 2A
	1125.447	1.244	32 ± 4	LiF 1B, LiF 2A
	1133.665	0.728	≤ 18	LiF 1B, LiF 2A
	1143.226	1.342	42 ± 5	LiF 1B, LiF 2A
	1144.938	2.096	92 ± 6	LiF 1B, LiF 2A
Fe III . .	1122.526	2.260	16 ± 5	LiF 1B, LiF 2A

^aVacuum wavelengths and oscillator strengths from Morton (in preparation).

^bEquivalent widths, 1σ errors, or upper limits are listed.

^cIncluding Galactic D I $\lambda 937.548$.

Table 5. Atomic Column Densities in the LLIV Arch

Species	I.P. [eV]	b [km s ⁻¹]	log N^a
H I	13.60	...	19.54 ± 0.01 ^b
C II	24.38	8	≤ 15.20
N I	14.53	8	15.25 ± 0.17
N II	29.60	8	14.39 ± 0.20
O I	13.62	8	16.42 ± 0.23
Si II	16.35	8	14.68 ± 0.15
P II	19.73	8	13.21 ± 0.12
Ar I	15.76	8	13.60 ± 0.07
Fe II	16.16	8	14.38 ± 0.05
Fe III	30.65	8	12.97 ± 0.10

^aThe 1σ column density errors listed for the metal lines do not include the systematic error associated with the possibility that the different species do not follow the curve of growth defined by Fe II.

^bFrom 21 cm emission line data with a beam size of 9'.1 centered on PG 0804+761.

Table 6. Normalized Gas Phase Abundances in the LLIV Arch

Element X	$\log(X/H)_{\odot}$ ^a +12.00	$[X/H I]$ ^b	$[X/(H I+H II)]$ ^c
C II	8.55
N I	7.97	-0.26 ± 0.17	...
N I+N II	7.97	...	-0.29 ± 0.20
O I	8.87	$+0.01 \pm 0.23$...
Si II	7.55	-0.41 ± 0.15	-0.50 ± 0.15
P II	5.57	$+0.10 \pm 0.12$	$+0.01 \pm 0.12$
Ar I	6.65	-0.59 ± 0.07	...
Fe II	7.51	-0.67 ± 0.05	...
Fe II+Fe III	7.51	...	-0.74 ± 0.05

^aAnders & Grevesse (1989); Grevesse & Noels (1993).

^b $[X/H I] = \log(N_X/N_{HI}) - \log(X/H)_{\odot}$.

^c $[X/(H I+H II)] = \log(N_X/N_{HI+H II}) - \log(X/H)_{\odot}$.

Table 7. Intergalactic Absorption Lines toward PG 0804+761^a

Species	$\lambda_{\text{obs}}^{\text{a}}$ [Å]	$z_{\text{abs}}^{\text{b}}$	W_{λ}^{c} [mÅ]	$\log N$
Intervening System ^d				
Ly β	1044.642	0.0185 ± 0.0004	73 ± 19	$14.00^{+0.10}_{-0.13}^{\text{g}}$
Associated System				
Ly γ	1072.050	0.1023 ± 0.0004	62 ± 12	$14.27^{+0.07}_{-0.10}^{\text{g}}$
Ly β	1130.605	0.1023 ± 0.0004	$172 \pm 11^{\text{e}}$	$14.37 \pm 0.03^{\text{g}}$
C III	1076.994	0.1023 ± 0.0017	... ^f	...
O VI	1137.483	0.1023 ± 0.0004	$108 \pm 8^{\text{e}}$	$14.04^{+0.03}_{-0.05}^{\text{h}}$
O VI	1143.613	0.1022 ± 0.0004	49 ± 7	$14.00^{+0.04}_{-0.05}^{\text{h}}$

^aThe unidentified absorption feature near 1142 Å (see Fig. 2) is most likely an instrumental artefact but not an intergalactic absorption line.

^bHeliocentric wavelengths.

^cVacuum wavelengths from Morton (in preparation).

^dEquivalent widths in the rest frame are listed.

^eO VI absorption at $z = 0.0185$ is not detected. 3σ upper limits for the two O VI lines at $\lambda_{\text{rest}} = 1031.926$ and 1037.617 Å are 64 and 52 mÅ, respectively.

^fTwo-component structure.

^gBlended by Galactic H₂ R(0),2-0.

^hColumn density calculated via $N = 1.13 \times 10^{17} W_{\lambda} / f \lambda_0^2$, assuming optically thin absorption.

ⁱColumn density calculated using apparent-optical-depth method (see Savage & Sembach 1991).